HHS Public Access

Author manuscript

Science. Author manuscript; available in PMC 2021 November 16.

Published in final edited form as:

Science. 2020 October 09; 370(6513): 247–250. doi:10.1126/science.abb4151.

Alternating sequences of future and past behavior encoded within hippocampal theta oscillations

Mengni Wang[1], **David J. Foster**[2], **Brad E. Pfeiffer**[1,*]

[1]Neuroscience Graduate Program, Department of Neuroscience, Peter O'Donnell Jr. Brain Institute, University of Texas Southwestern Medical Center, Dallas, TX 75390, USA.

[2]Department of Psychology and Helen Wills Neuroscience Institute, University of California, Berkeley, CA 94720, USA.

Abstract

Neural networks display the ability to transform forward-ordered activity patterns into reverse-ordered, retrospective sequences. The mechanisms underlying this transformation remain unknown. We discovered that, during active navigation, rat hippocampal CA1 place cell ensembles are inherently organized to produce independent forward- and reverse-ordered sequences within individual theta oscillations. This finding may provide a circuit-level basis for retrospective evaluation and storage during ongoing behavior. Theta phase procession arose in a minority of place cells, many of which displayed two preferred firing phases in theta oscillations and preferentially participated in reverse replay during subsequent rest. These findings reveal an unexpected aspect of theta-based hippocampal encoding and provide a biological mechanism to support the expression of reverse-ordered sequences.

Experience necessarily occurs in a sequential manner, and hippocampal function is critical for representation and storage of sequential information. Adaptive behavior requires the ability to analyze experience, both prospectively and retrospectively. It remains unclear how forward-ordered neural activity can facilitate storage or expression of reverse-ordered sequences, which are observed in ripple-based reverse replay (1, 2) and may underlie human episodic memory retrieval (3). Accurate, precise, and stable spatial representation across the hippocampal network of place cells is insufficient to support goal-directed spatial navigation in the absence of theta oscillations (4, 5). This indicates that the precise, population-level patterns of activity organized by theta oscillations, termed theta sequences (6–9), are critical for hippocampal-dependent, memory-guided behavior (10). We examined

*Corresponding author. brad.pfeiffer@utsouthwestern.edu.

Author contributions: B.E.P. and D.J.F. conceived the original experiments. B.E.P. performed the original experiments and collected the original data. M.W. and B.E.P. conceived, designed, and performed the analyses. M.W. and B.E.P. wrote the manuscript.

Competing interests: None declared.

SUPPLEMENTARY MATERIALS

science.sciencemag.org/content/370/6513/247/suppl/DC1

Materials and Methods

Figs. S1 to S18

Table S1

References (36–38)

MDAR Reproducibility Checklist

ensemble place cell activity recorded from bilateral hippocampal area CA1 in rats engaged in reward-seeking exploration of both linear tracks and open arenas (11, 12). Large numbers of simultaneously monitored place cells (per-session mean ± SEM = 144.3 ± 14.0 putative excitatory units) allowed a memoryless, uniform-prior Bayesian decoding algorithm to accurately extract the spatial information encoded by the recorded ensemble in each session (table S1). We investigated the temporally compressed spatial trajectories expressed within theta oscillations during active exploration (speed ≥10 cm/s), examining a total of 115,845 theta oscillations (7240.3 ± 1126.7 per session).

We quantified sequential spatial representation within theta sequences by aligning each decoded time frame to the rat's current movement direction every 5 ms. Theta sequences in both the linear track and open field tasks typically produced a virtual spatial path progressing from the rat's current location ahead of the animal during periods of active movement (Fig. 1A and figs. S1 and S2). However, theta oscillations rarely progressed uniformly in a single direction. They consisted of two distinct components, one that traveled ahead of the rat and a second that moved backward in the reverse direction of the animal's actual movement (Fig. 1, A and B, and figs. S1 and S2). The reverse component consistently occurred near the peak of theta oscillation (Fig. 1B), a time window associated with minimal hippocampal population activity (6). To ensure that the observation of a backward theta sequence was not a trivial result of low spike counts biasing the decoding algorithm, we initially restricted our analysis to the third of theta oscillations in each session with the highest firing rates within that window. On the basis of troughs in posterior probability distributions (Fig. 1B), we defined two windows in the theta oscillation: a forward window from phases 250° to 420°/60° and a reverse window from 80° to 230°, associated with statistically significant forward and backward virtual trajectories, respectively (Fig. 1C and figs. S3 and S4). Virtual representations of forward or reverse trajectories were observed within single theta oscillations (fig. S5) and were directly and independently correlated with population activity in the forward or reverse windows, respectively (fig. S6). The reverse component of the theta sequence was not a trivial consequence of our analysis methods or resetting of the forward trajectory (figs. S7 and S8).

Taking advantage of the fact that place cells display direction-selective firing patterns on linear tracks (13), we observed that both the forward and reverse components were predominantly encoded by neurons representing the rat's current movement direction (Fig. 1, D and E, and fig. S2). Thus, the reverse component of a theta sequence bears a direction-momentum relationship consistent with the rat running backward rather than turning around and running forward in the opposite direction. The direction-momentum relationship in reverse theta sequences thus bears a similarity to reverse replay observed within rest-based sharp-wave ripples (1, 2).

Given that the reverse window was confined to phases of the theta oscillation associated with minimal firing across the hippocampal network, we investigated whether the backward portion of the theta sequence was encoded by a different population of neurons than the forward component—a population that might selectively fire while the remainder is relatively silent. Although most neurons (which we termed "unimodal cells") displayed a canonical (6) unimodal relationship between firing rate and theta phase, a subset of neurons

("bimodal cells") displayed a bimodal relationship with theta phase (Fig. 2, A and B, and fig. S9), consistent with the firing patterns reported for deep CA1 pyramidal neurons (14). The activity of bimodal cells across the theta oscillation was separated into two windows: a major peak between phases 200° and 430°/70°, comparable to the forward window, and a minor peak between 80° and 190°, consistent with the reverse window (Fig. 2B). Spatial representation during the reverse window, but not the forward window, was more strongly influenced by bimodal cell activity as opposed to unimodal activity (fig. S10). Bimodal cells were more likely to fire in ripples than unimodal cells (Fig. 2C) and further displayed an increased likelihood to participate in reverse replay as opposed to forward replay (Fig. 2D), indicating a neuronal link between reverse theta sequences and reverse replay. Bimodal cells had similar cluster quality measurements to those of unimodal cells (figs. S11 and S12) and were thus unlikely to be a trivial consequence of poor single-unit isolation. Similar to deep CA1 pyramidal neurons (15), bimodal cells were more likely to shift their preferred phase of firing within theta during REM (rapid eye movement) sleep (fig. S13). Furthermore, like deep CA1 neurons (16), bimodal cells displayed increased spatial information (fig. S12).

We next sought to identify the cellular mechanism that produces the reverse component of theta sequences. The predominant model accounting for the well-studied forward component of theta sequences is theta phase precession (6, 7), the iterative firing of a place cell at progressively earlier phases of the theta oscillation as the rat passes through the neuron's firing field (17). We reasoned that the backward trajectory encoded within theta sequences may be explained by the opposite process: phase procession within individual place cells during the reverse window. When we examined the relationship of theta firing phase to the rat's location within each cell's place field, we identified clear phase precession during the major peak of activity for both unimodal and bimodal cells (Fig. 3, A and B, and fig. S14). However, during the minor peak of activity associated with the reverse window, many bimodal cells displayed significant phase procession (Fig. 3C and figs. S14 and S15). The average phase-versus-location plots for bimodal cells contained two distinct clusters rather than the single linear or curved relationship observed for unimodal neurons (Fig. 3B), as indicated in earlier work (6, 18). Although their total firing rates were lower in the minor peak window, unimodal cells also displayed phase procession within this period (Fig. 3, B and C, and figs. S14 and S15). Thus, phase procession during the reverse window is not a characteristic aspect of bimodal cells but is likely a common feature of hippocampal activity during this time frame.

Finally, we sought to identify whether the forward and reverse theta sequences were driven by a common source or were instead regulated by independent inputs. Because forward and reverse sequences were respectively correlated with population activity during the forward and reverse windows (fig. S6), we reasoned that if a common input accounted for both the forward and reverse components, population activity in both windows would be strongly correlated. If forward and reverse theta sequences were instead driven by two distinct inputs, activity in these two windows should be independent. Neural activity within the major peak, but not the minor peak, positively correlated with the power of the hippocampal theta oscillation (Fig. 4 and fig. S16). Activity at the minor peak, but not the major peak, was correlated with the power of the beta oscillation (Fig. 4 and fig. S16). In addition, beta power was increased in theta oscillations expressing reverse theta sequences (fig. S17). Although

some prior studies suggest that the hippocampus may receive both theta-frequency and beta-frequency inputs (19–21), several others indicate that two independent theta-frequency inputs that are roughly antiphase to one another drive activity in area CA1 (14, 22–24), which can produce beta-frequency oscillatory activity. Our data are consistent with the second model (fig. S18) and support the hypothesis that activity in the forward and reverse windows is driven by two independent, antiphase theta-frequency inputs.

CA1 pyramidal neurons receive two primary, anatomically segregated excitatory inputs: the Shaffer collaterals originating in hippocampal area CA3 and the perforant path from layer 3 of the entorhinal cortex (EC3). The timing of these respective inputs is also segregated, with EC3 input arriving near the peak of CA1 theta oscillation (during the reverse window) and CA3 input arriving nearer the trough of CA1 theta oscillation (during the forward window) (14, 22). Thus, the relative timing and independent expression that we observe in the forward and reverse components of theta sequences indicate that CA3 input selectively facilitates phase precession and drives the forward, prospective sequence, whereas antiphase EC3 input selectively facilitates phase procession and drives the reverse, retrospective sequence. Consistent with this interpretation, theta oscillations with significant reverse sequences have increased power in the fast and medium gamma bands (fig. S17), which is associated with EC input to CA1 (14, 25), but not the slow gamma band, which is associated with CA3 input (25).

Although several models have been proposed to explain the observation of reverse replay (1, 26, 27), it remains unclear how reverse-ordered sequences can arise from forward-ordered activity. Given that activity within the reverse window is linked to participation in reverse replay events (Fig. 2D), our data suggest that synaptic inputs arriving during this window, likely originating from EC3, facilitate synaptic changes across the hippocampal network that underlie the expression of reverse replay. CA1 synapses receiving input from area CA3 have synaptic and plastic properties that are distinct from those of synapses receiving input from EC3 (28, 29). The relative timing of EC3 input also affects plasticity at Shaffer collateral synapses (30, 31). The increased likelihood of observing reverse replay immediately after a behavioral trajectory (2) and the lower level of reverse replay reported during sleep (32) suggest that plasticity generated in the reverse window may be stronger but more temporary than plasticity generated in the forward window. The power of a beta-frequency oscillation, which we show to be correlated with the reverse theta sequence (Fig. 4 and figs. S16 and S17), is increased during early exploration of novel environments (20) and may represent enhanced EC3 input, which facilitates the rapid expression of reverse replay (1).

Although most studies of theta sequences have reported exclusively forward-ordered trajectories (6, 7), a small number have suggested the presence of retrospective information encoded within some hippocampal theta oscillations (8, 32–34). Most prior studies lacked the cell yield necessary to accurately quantify spatial sequences on a fine time scale. They were thus unable to observe the consecutive, phase-locked forward and reverse sequences we report here, particularly during the reverse window when population activity is low. Bimodal firing rates and theta phase–versus–location relationships of individual neurons have been previously reported (6, 14, 18). However, these earlier studies did not predict sequential representation of prior experience within individual theta oscillations. Finally, a

recent study reported that the forward component of successive theta sequences alternates between possible future paths or heading directions during phases of theta that correspond to the forward window (9). Although these findings align with our observations, a notable contrast is that here we have specifically identified two distinct and independent information streams within each theta cycle: one that represents a possible future outcome and one that represents prior behavior in the reverse order. Our findings therefore facilitate understanding and integration of prior work into a broad, cohesive model of hippocampal circuit function, demonstrating alternating prospective and retrospective evaluation of behavior within individual theta oscillations.

Supplementary Material

Refer to Web version on PubMed Central for supplementary material.

ACKNOWLEDGMENTS

Funding:

This work was supported by NIH R01-MH085823, NIH R01-NS104829, the Alfred P. Sloan Foundation, and the Southwestern Medical Foundation.

Data and materials availability:

Data analysis code (MATLAB) is available on GitHub (github.com/Brad-E-Pfeiffer/ThetaForwardReverseCode) and Zenodo (35). All (other) data needed to evaluate the conclusions in the paper are present in the paper or the supplementary materials.

REFERENCES AND NOTES

1. Foster DJ, Wilson MA, Nature 440, 680–683 (2006). [PubMed: 16474382]
2. Diba K, Buzsáki G, Nat. Neurosci 10, 1241–1242 (2007). [PubMed: 17828259]
3. Wimmer GE, Liu Y, Vehar N, Behrens TEJ, Dolan RJ, Nat. Neurosci 23, 1025–1033 (2020). [PubMed: 32514135]
4. Robbe D, Buzsáki G, J. Neurosci 29, 12597–12605 (2009). [PubMed: 19812334]
5. Bolding KA, Ferbinteanu J, Fox SE, Muller RU, Hippocampus 30, 175–191 (2020). [PubMed: 31301167]
6. Skaggs WE, McNaughton BL, Wilson MA, Barnes CA, Hippocampus 6, 149–172 (1996). [PubMed: 8797016]
7. Dragoi G, Buzsáki G, Neuron 50, 145–157 (2006). [PubMed: 16600862]
8. Gupta AS, van der Meer MA, Touretzky DS, Redish AD, Nat. Neurosci 15, 1032–1039 (2012). [PubMed: 22706269]
9. Kay K et al., Cell 180, 552–567.e25 (2020). [PubMed: 32004462]
10. Drieu C, Todorova R, Zugaro M, Science 362, 675–679 (2018). [PubMed: 30409880]
11. Pfeiffer BE, Foster DJ, Nature 497, 74–79 (2013). [PubMed: 23594744]
12. Pfeiffer BE, Foster DJ, Science 349, 180–183 (2015). [PubMed: 26160946]
13. McNaughton BL, Barnes CA, O'Keefe J, Exp. Brain Res 52, 41–49 (1983). [PubMed: 6628596]
14. Fernández-Ruiz A et al., Neuron 93, 1213–1226.e5 (2017). [PubMed: 28279355]
15. Mizuseki K, Diba K, Pastalkova E, Buzsáki G, Nat. Neurosci 14, 1174–1181 (2011). [PubMed: 21822270]
16. Danielson NB et al., Neuron 91, 652–665 (2016). [PubMed: 27397517]

17. O'Keefe J, Recce ML, Hippocampus 3, 317–330 (1993). [PubMed: 8353611]
18. Yamaguchi Y, Aota Y, McNaughton BL, Lipa P, J. Neurophysiol 87, 2629–2642 (2002). [PubMed: 12037166]
19. Lansink CS et al., J. Neurosci 36, 10598–10610 (2016). [PubMed: 27733611]
20. Berke JD, Hetrick V, Breck J, Greene RW, Hippocampus 18, 519–529 (2008). [PubMed: 18398852]
21. Rangel LM, Chiba AA, Quinn LK, Front. Syst. Neurosci 9, 96 (2015). [PubMed: 26190979]
22. Schomburg EW et al., Neuron 84, 470–485 (2014). [PubMed: 25263753]
23. Valero M, de la Prida LM, Curr. Opin. Neurobiol 52, 107–114 (2018). [PubMed: 29729527]
24. Navas-Olive A et al., Nat. Commun 11, 2217 (2020). [PubMed: 32371879]
25. Colgin LL et al., Nature 462, 353–357 (2009). [PubMed: 19924214]
26. Koene RA, Hasselmo ME, Neural Netw 21, 276–288 (2008). [PubMed: 18242057]
27. Haga T, Fukai T, eLife 7, e34171 (2018). [PubMed: 29969098]
28. Arrigoni E, Greene RW, Br. J. Pharmacol 142, 317–322 (2004). [PubMed: 15155538]
29. Aksoy-Aksel A, Manahan-Vaughan D, Front. Synaptic Neurosci 5, 5 (2013). [PubMed: 23986697]
30. Takahashi H, Magee JC, Neuron 62, 102–111 (2009). [PubMed: 19376070]
31. Basu J et al., Science 351, aaa5694 (2016). [PubMed: 26744409]
32. Wikenheiser AM, Redish AD, Hippocampus 23, 22–29 (2013). [PubMed: 22736562]
33. Bieri KW, Bobbitt KN, Colgin LL, Neuron 82, 670–681 (2014). [PubMed: 24746420]
34. Cei A, Girardeau G, Drieu C, Kanbi KE, Zugaro M, Nat. Neurosci 17, 719–724 (2014). [PubMed: 24667574]
35. Wang M, Foster D, Pfeiffer B, Data from "Alternating sequences of future and past behavior encoded within hippocampal theta oscillations," Zenodo (2020); doi:10.5281/zenodo.3972156.

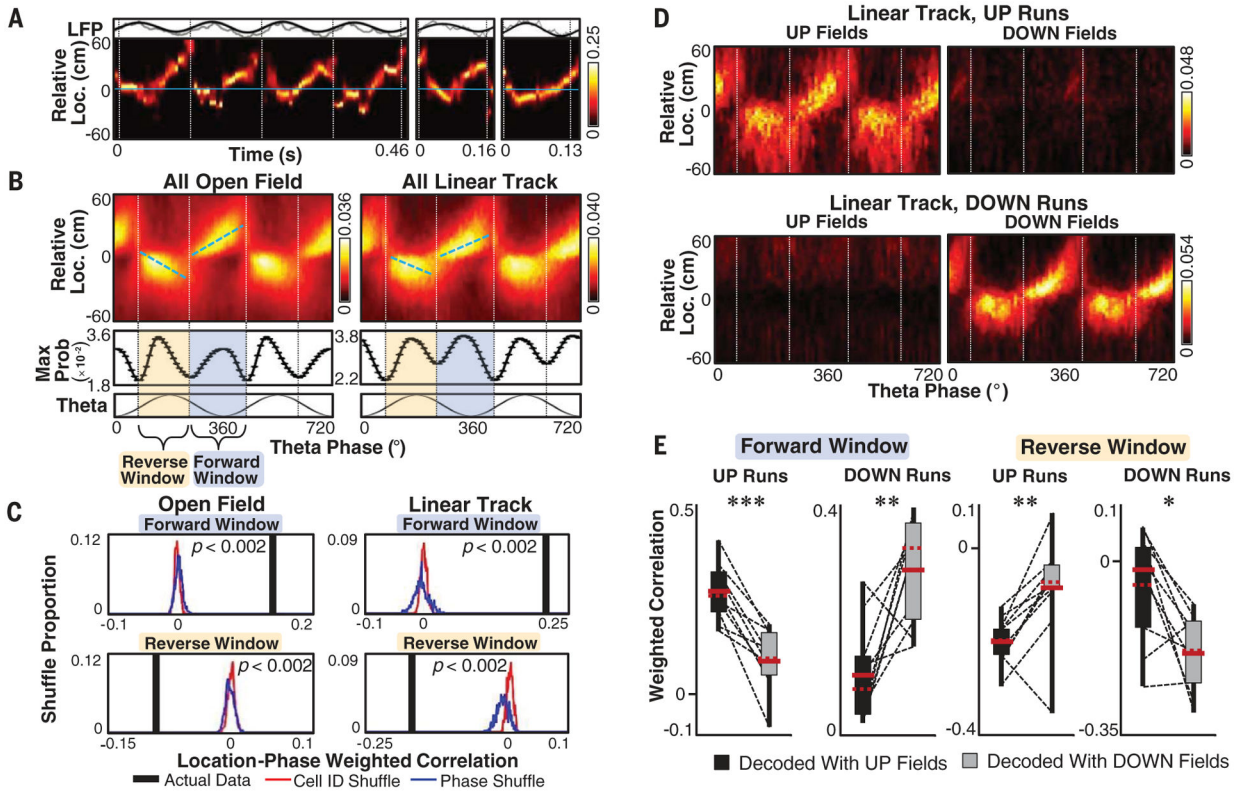

Fig. 1. Forward and reverse components of theta sequences.

(**A**) Examples of theta sequences displaying both reverse and forward components. (Top) Raw (gray) and theta-filtered (black) local field potential (LFP) trace. Loc., location. (Bottom) Decoded spatial representation probability relative to the rat's current location (blue line) and movement direction (positive values). Dashed lines mark the 70° theta phase. (**B**) (Top) Across-session probability histogram of theta phase (10° bins) with maximum posterior probability at each position relative to rat position (2-cm bins) for the third of theta oscillations with highest firing near the peak of theta phase. Dashed blue lines indicate best fit (least-squares method). (Middle) Smoothed (Gaussian, $\sigma = 10°$) maximum value of each theta bin above. Vertical dashed lines indicate troughs in maximum probability (Max Prob) density (70° and 240°) used to define forward and reverse windows. (Bottom) Idealized theta oscillation. (**C**) Actual data and distribution of weighted correlation values for 500 theta phase or cell ID shuffles per theta oscillation in forward and reverse windows. The maximum Monte-Carlo *P* value for either shuffle displayed is noted. (**D**) As in the top portion of (B), but for only linear track sessions separated by runs across the track in the UP (top) or DOWN (bottom) direction, decoded with place fields calculated during up (left) or down (right) runs. (**E**) Per-session box-and-whisker plot (box, quartile; whiskers, extreme range), mean (red solid line), and median (red dashed line) of weighted correlations per session for forward and reverse windows during up or down runs decoded with up or down fields. Dashed lines represent individual session averages. $*P < 0.05$, $**P < 0.01$, $***P < 0.001$; Wilcoxon rank-sum test; $n = 10$ sessions.

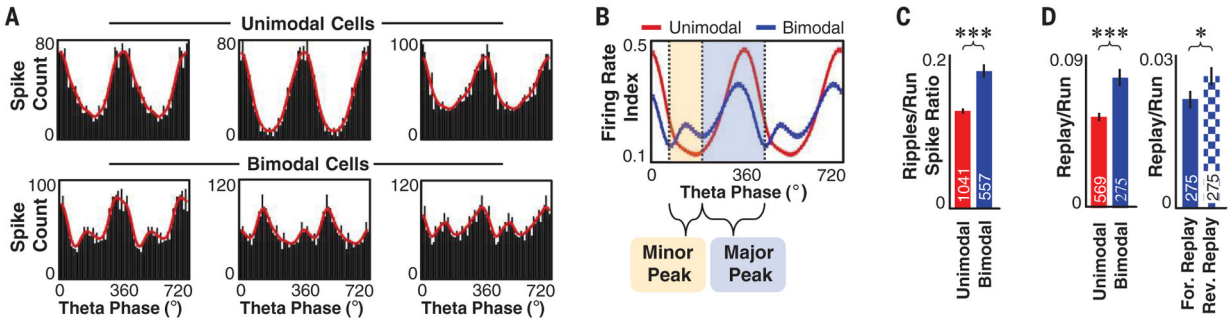

Fig. 2. Unimodal and bimodal cells.

(**A**) Raw (black) and smoothed (red) histograms of action potential count per theta phase for example unimodal (top) and bimodal (bottom) cells. (**B**) Mean ± SEM firing rate index versus theta phase for all unimodal (red; $n = 1041$) and bimodal (blue; $n = 557$) cells across all open field and linear track sessions. Vertical lines mark troughs of mean firing for bimodal cells used to separate theta oscillations into major and minor peak windows. (**C**) Mean ± SEM ratio of spikes emitted across all ripples to spikes emitted during runs (velocity ≥10 cm/s) for unimodal or bimodal cells across all sessions. (**D**) (Left) Mean ± SEM ratio of spikes in significant replay events to spikes during runs for unimodal or bimodal cells across all linear track sessions. (Right) Mean ± SEM ratio of spikes in forward (solid) or reverse (checkered) replay to spikes during runs for bimodal cells across all linear track sessions. $*P < 0.05$, $***P < 0.001$; Student's t test; cell number (n) is listed on the bar graphs.

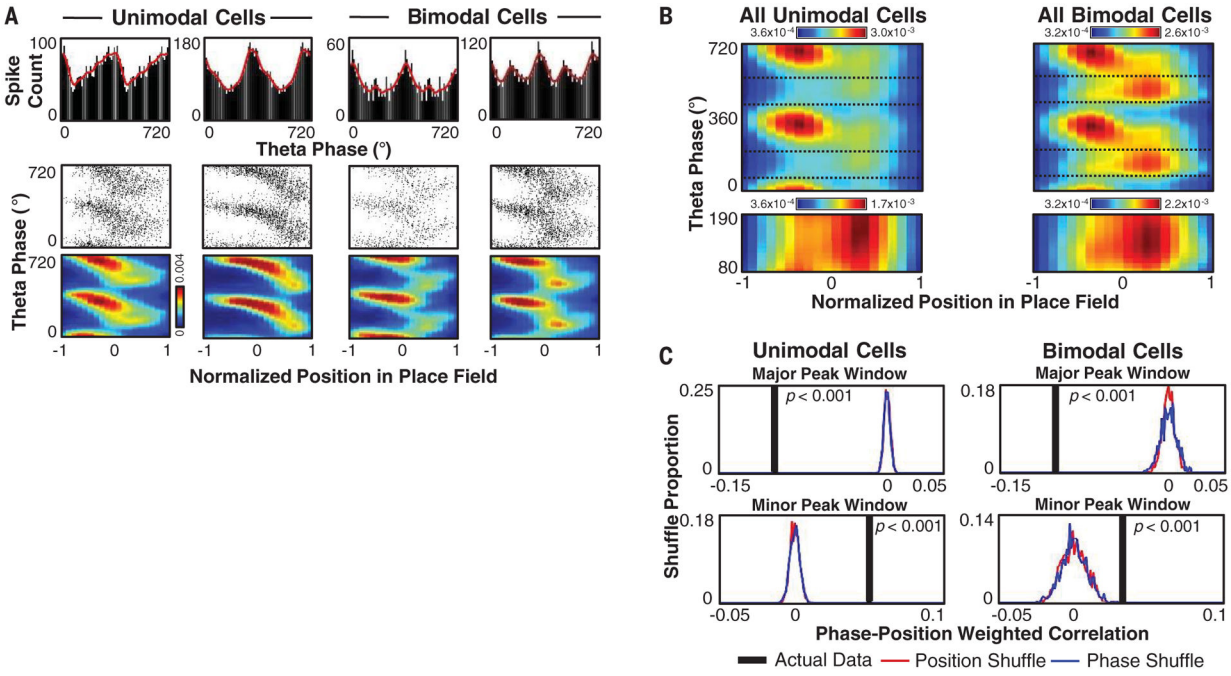

Fig. 3. Phase precession and procession.

(**A**) Example unimodal and bimodal cells displaying phase precession and/or phase procession. (Top) Spike count per theta phase. (Bottom) Spike plot and smoothed (Gaussian, $\sigma = 2$ bins) probability heatmap of theta phase versus normalized location (−1 is entering the field, 1 is leaving). (**B**) (Top) Smoothed firing probability per theta phase bin (10°) and normalized position in place field bin (0.1), averaged across all cells for open field and linear track sessions. Dotted lines mark major and minor peak boundaries. (Bottom) As in top panel, but showing only the minor peak window with a rescaled colormap. (**C**) Actual data and distribution of weighted correlation values for 1000 shuffles of position or theta phase in major peak and minor peak windows. The maximum Monte-Carlo *P* value for either shuffle displayed is noted.

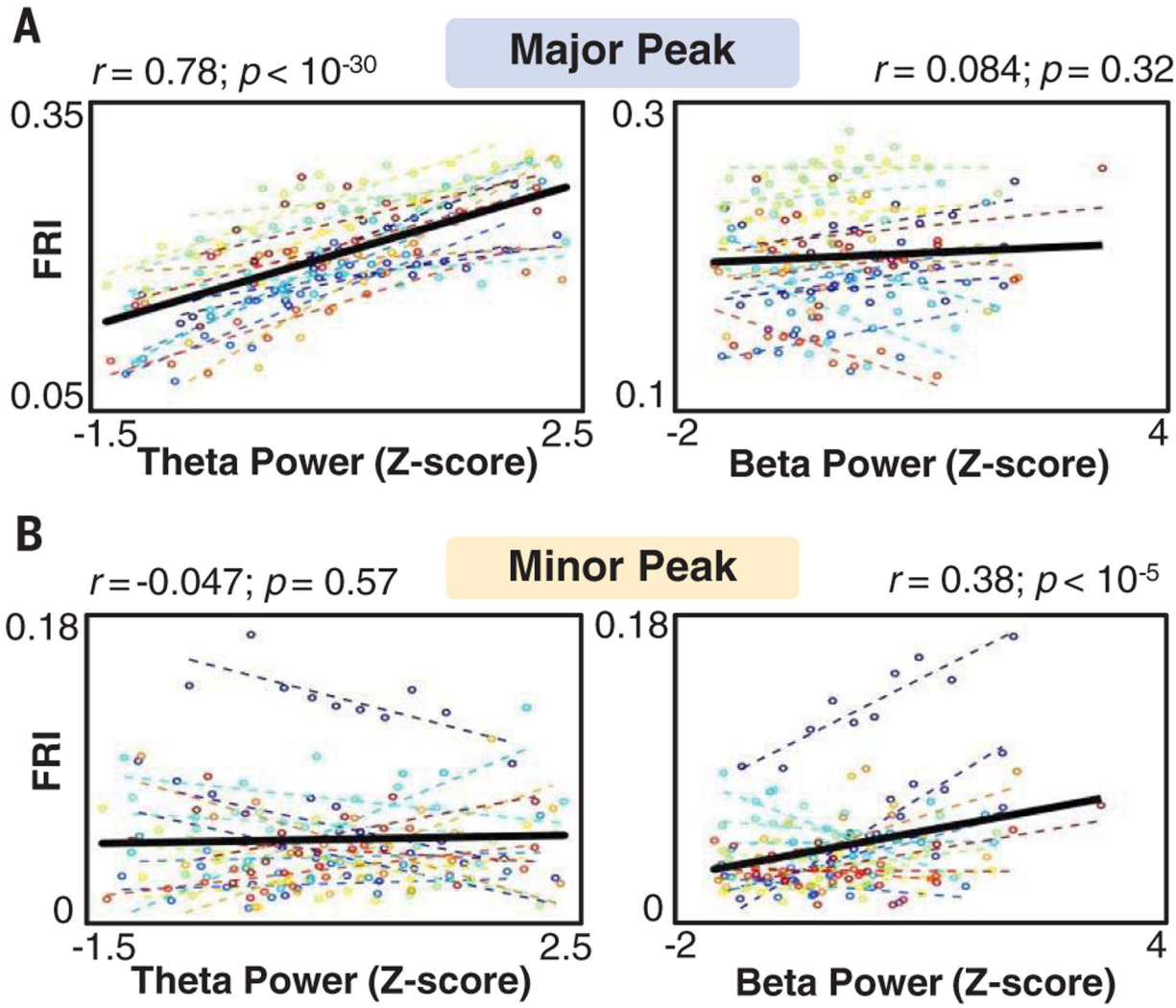

Fig. 4. Independent activity in forward and reverse components of theta sequences.

For all open field and linear track sessions, firing rate index (FRI) in the major peak window (**A**) or minor peak window (**B**) as a function of theta (6 to 12 Hz) power (left) or beta (15 to 20 Hz) power (right), separated into 10 divisions per session. Colored lines indicate data and best fit for each session; black lines indicate best fit across all sessions. Statistics are based on repeated measures of correlation; $n = 16$ sessions.